

Low-Dose CT Image Reconstruction by Fine-Tuning a UNet Pretrained for Gaussian Denoising for the Downstream Task of Image Enhancement

Tim Selig, Thomas März, Martin Storath and Andreas Weinmann

Abstract—Computed Tomography (CT) is a widely used medical imaging modality, and as it is based on ionizing radiation, it is desirable to minimize the radiation dose. However, a reduced radiation dose comes with reduced image quality, and reconstruction from low-dose CT (LDCT) data is still a challenging task which is subject to research. According to the LoDoPaB-CT benchmark, a benchmark for LDCT reconstruction, many state-of-the-art methods use pipelines involving UNet-type architectures. Specifically the top ranking method, ItNet, employs a three-stage process involving filtered backprojection (FBP), a UNet trained on CT data, and an iterative refinement step. In this paper, we propose a less complex two-stage method. The first stage also employs FBP, while the novelty lies in the training strategy for the second stage, characterized as the CT image enhancement stage. The crucial point of our approach is that the neural network is pretrained on a distinctly different pretraining task with non-CT data, namely Gaussian noise removal on a variety of natural grayscale images (photographs). We then fine-tune this network for the downstream task of CT image enhancement using pairs of LDCT images and corresponding normal-dose CT images (NDCT). Despite being notably simpler than the state-of-the-art, as the pretraining did not depend on domain-specific CT data and no further iterative refinement step was necessary, the proposed two-stage method achieves competitive results. The proposed method achieves a shared top ranking in the LoDoPaB-CT challenge and a first position with respect to the SSIM metric.

Index Terms—Computed Tomography, Image Reconstruction, Machine Learning, UNet.

1 INTRODUCTION

Computed tomography (CT) is a cornerstone of modern medical imaging, providing accurate and non-invasive visualization of the internal structures of the human body. Its widespread use is due to its versatility, as it serves as a diagnostic tool for a wide range of medical examinations [1], [2]. Despite a long history of contributions, the reconstruction of CT images remains an active area of research due to the continuous search for higher image quality, less artifacts and reduced noise while at the same time reducing the ionizing radiation [3]. In particular, reconstruction from low radiation dose projections and reconstruction from sparse or limited projection data remain challenging tasks. This work is focused on low-dose CT (LDCT) reconstruction, which is subject to intensive research, see e.g. [4], [5], [6], [7], [8], [9], [10].

Until a few years ago, reconstructions from iterative variational regularization methods were among the state-of-the-art for CT image reconstruction; for example, these methods are based on total variation [11], total generalized varia-

tion [12] or Hessian Schatten norms [13] regularization, to mention only a few. In recent years, deep learning methods have led to a paradigm shift in medical image reconstruction. In particular, convolutional neural networks (CNNs) have demonstrated convincing capabilities in mitigating artifacts and reconstruction noise [14]. One may distinguish between fully learned methods, iterative approaches, and multi-stage methods. Fully learned methods involve the direct reconstruction of images through deep learning architectures, utilizing raw projection data or sinograms as input. Iterative approaches, such as statistical iterative reconstruction or model-based iterative reconstruction (MBIR) aim at refining image quality [15] by alternating between reconstruction and denoising. Several studies employing MBIR techniques, including the Plug-and-Play framework for the integration of deep learning-based denoisers, have consistently showcased substantial improvements in image quality, robustness to noise, and overall enhancement of the medical image reconstruction process [16], [17]. Two-stage and Multi-stage methods employ neural networks as a step or as steps in a pipeline to improve the results of an initial reconstruction. Typically, filtered backprojection (FBP) is utilized in the initial reconstruction phase. In a subsequent stage, or in subsequent stages, neural networks are employed to perform image enhancement tasks which improve the reconstruction quality. Examples for this class of methods are the UNet++ [18], the ISTA UNet [19] as well as ItNet [20] discussed in more detail below. Also the approach proposed in this paper falls into this category.

Tim Selig is with the Computer Vision, Imaging and Data Analysis Group, Hochschule Darmstadt, 64287 Darmstadt, Germany (tim.selig@h-da.de) and also with the Lab for Mathematical Methods in Computer Vision and Machine Learning, Technische Hochschule Würzburg-Schweinfurt, 97421 Schweinfurt, Germany.

Thomas März and Andreas Weinmann are with the Computer Vision, Imaging and Data Analysis Group, Hochschule Darmstadt, 64287 Darmstadt, Germany (thomas.maerz@h-da.de, andreas.weinmann@h-da.de).

Martin Storath is with the Lab for Mathematical Methods in Computer Vision and Machine Learning, Technische Hochschule Würzburg-Schweinfurt, 97421 Schweinfurt, Germany (martin.storath@thws.de).

For the quantitative evaluation of the reconstruction from LDCT images, the LoDoPaB-CT challenge has been established by Leuschner et al. [21]. The dataset consists of pairs of LDCT images and corresponding normal-dose CT (NDCT) images. In the corresponding LoDoPaB-CT challenge the top ranking methods are mostly based on deep neural networks, including the ISTA UNet [19], the Learned Primal-Dual algorithm [22], Multiscale UNet-like Sparse Coding (MUSC) [23] and ItNet [20]. ISTA UNet, an adaptation of the UNet architecture, replaces the encoder with a sparse representation and linearizes the decoder. The Learned Primal-Dual algorithm optimizes the parameters of the Primal-Dual optimization algorithm through a data-driven approach. MUSC enhances a UNet-like architecture with multiscale convolutional dictionaries and sparse coding, increasing its capacity to capture fine details. The currently top ranking method, ItNet (short for iterative network), is a three-stage method consisting of FBP, a pre-trained UNet and an iterative refinement step.

Recently, there is a trend in Computer Vision (originating from Natural Language Processing) to pretraining deep neural networks on a “pretrain” task on a large dataset (from potentially different fields of applications), and then to fine-tune this network for a downstream task; cf., e.g., [24] in the context of Natural Language Processing and [25] in the context of Computer Vision. Our proposed method uses this strategy within a two-stage approach for LDCT reconstruction.

1.1 Proposed Approach

We propose a two-stage method for LDCT reconstruction. It consists of an initial reconstruction by classical FBP and a CT image enhancement stage. The novelty lies in the training strategy of the second stage: we exploit the pretraining achieved through a distinct training task, specifically the removal of Gaussian noise from natural grayscale images (photographs). In particular, we employ the DRUNet model described in the work by Zhang et al. [17], originally developed as a Gaussian denoiser for natural grayscale and color images within a Plug-and-Play framework and trained on a self-constructed dataset, consisting of images from the Berkeley segmentation dataset, Waterloo Exploration Database, DIV2K dataset and Flick2K dataset. We then adapt it for the enhancement of FBP-reconstructed CT images. The adaptation includes a different loss function, adjusting the input and output dimensions, and data augmentation. We emphasize that the pretraining of the DRUNet uses a different class of images, and a different task, namely Gaussian denoising, whereas the downstream task of CT image enhancement is trained on FBP images with a non-Gaussian noise model. The fine-tuning with regard to the downstream task is performed with the LoDoPaB-CT dataset [26]. A visual representation of this sequential process is provided in Figure 1. The figure illustrates the two-stage process, involving FBP reconstruction and an optimization task with a SSIM-based loss function. To improve the robustness of the model we use two data augmentation techniques, namely adding Gaussian noise and rotating the input and ground truth images in all four major directions to make the model equivariant with respect to these transformations.

We emphasize that two-stage methods based on UNets or other deep neural networks are frequently used for CT image processing, e.g. [9], [10], [19], [23], [26], [27]. The distinctive feature of the proposed two-stage method is the training strategy which uses pretraining on non-CT images with a different noise characteristics than LDCT images.

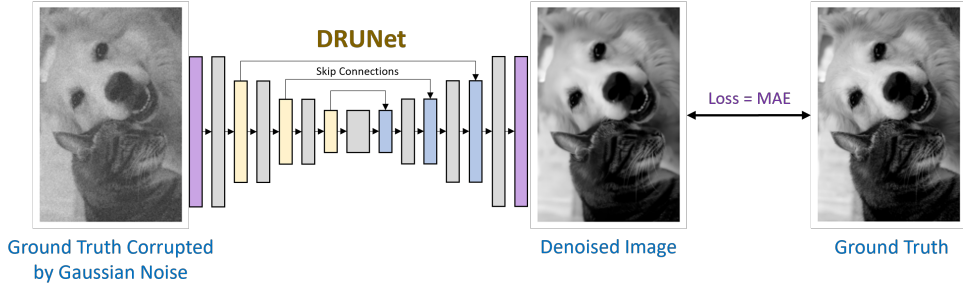
In the LoDoPaB-CT challenge for LDCT reconstruction [21], our proposed method currently holds the joint first place alongside ItNet [20]. Our method has the highest rank in the SSIM metric, but ItNet has a slight edge in the other three metrics, namely PSNR, PSNR-FR and SSIM-FR. Our approach shares similarities with ItNet as both employ FBP and a UNet as fundamental building blocks. But, there are also crucial differences: first, ItNet relies on a third iterative refinement stage, whereas the proposed method has only two stages. Second, the pretraining of ItNet uses pairs of sinogram and CT reconstructions, whereas the proposed method relies on pretraining a Gaussian denoiser on natural grayscale images. Therefore, the proposed method is structurally simpler than ItNet, and the pretraining did not rely on domain-specific data.

1.2 Related Work

The original *UNet* was introduced by Ronneberger et al. [28], which found widespread utilization for medical image processing. However, its applications extend beyond the medical domain. In non-medical scenarios, UNets have proven effective, as demonstrated in works such as [29], [30], [31]. UNet++, developed by Zhou et al. [18], enhances the capabilities of the original UNet. While the original UNet employs a basic architecture with skip connections, UNet++ introduces nested and dense convolution blocks to address the limitation of combining semantically dissimilar feature maps. UNet++ aims to progressively capture fine-grained details through these innovations. Furthermore, variations in loss functions, optimization techniques, and training strategies across the networks are described in [18]. Liu et al. introduce the ISTA UNet [19], an adaptation based on the encoder-decoder structure of the original UNet, that leverages task-driven dictionary learning and sparse coding. Unlike the original UNet, ISTA UNet replaces the encoder with a sparse representation and linearizes the decoder, showcasing versatility across datasets with sensitivity to hyperparameter choices. Pelt et al. [27] use a Mixed-Scale Dense CNN (MS-D-CNN) to exploit a variety of receptive fields to improve reconstruction accuracy. Continuing on the path of architectural innovations, Liu et al. introduce a multiscale UNet-like sparse coding (MUSC) approach in [23], exploring the development of multiscale convolutional dictionaries. Xiong et al. introduce Re-UNet, a novel reverse U-shaped network design [10], motivated by the need for enhancing LDCT image quality. Addressing the limitations of conventional UNet-based models, Re-UNet employs a unique upsampling-downsampling approach, aiming to preserve intricate texture details crucial for medical CT images. Additionally, Mazandarani et al. contribute to LDCT denoising with their UNeXt architecture, integrating modified ConvNeXt blocks into a UNet model [9].

The integration of encoder-decoder-based architectures and Generative Adversarial Networks (GANs) have also

Pretraining: Gaussian Denoiser on Natural Grayscale Images (Photographs)



Downstream Task: Two-Stage Process for LDCT Image Enhancement

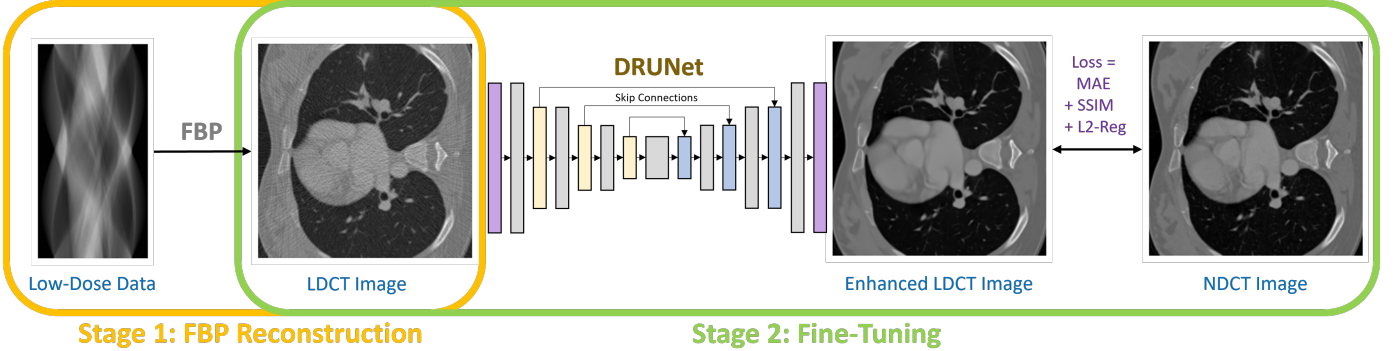


Fig. 1: Methodology Overview. The proposed approach consists of a two-stage process for LDCT image enhancement. First, a DRUNet is pretrained for Gaussian denoising of natural grayscale images. Second, the DRUNet is fine-tuned for the downstream task, i.e., for the enhancement of CT-images obtained from the FBP-stage.

received considerable attention in CT image reconstruction. For example Chen et al. [32] introduce a residual encoder-decoder architecture that mitigates the limitations associated with LDCT imaging. Similarly, Yang et al. [3] explore GAN-based denoising strategies, by leveraging the power of adversarial training to enhance the overall image quality. The literature in this field is extensive, as shown by the numerous publications [33], [34], [35], [36], [37], [38], [39].

Further progress in the field of reconstruction has been made through a variety of strategies. Wang et al. [8] introduce a convolution-free vision transformer, showcasing transformer adaptability. Liang et al. [40] combine edge enhancement with densely connected networks and compound loss functions. Denker et al. [41] connect traditional normalization with conditional variations to improve reconstruction. Kang et al. [42] employ directional wavelets for enhanced quality. Furthermore, the approach of Gholizadeh-Ansari et al. [43] integrate edge detection layers and perceptual loss functions. In addition, Li et al. [7] utilize double enhancement layers within a transformer architecture, highlighting the versatility of transformers in enhancing LDCT image quality.

2 METHODOLOGY

In this section, we present the technical details of the proposed approach to CT image reconstruction. We outline the mathematical framework underlying our methodology and describe the key components, including the deep neural

network architecture, the process of fine-tuning and the adaption of the network.

2.1 Problem Formulation

CT imaging is the task of reconstructing a high-quality CT image from raw projection data obtained through X-ray measurements from various angles. The forward model of this process describes the relationship between the acquired projection data and the desired image. Let y denote the raw projection data acquired by the imaging system, $x \in \mathbb{R}^{n \times n}$ represents the true CT image, and R denotes the (discrete) Radon transform that models the X-ray attenuation process [44]. Then, the forward model can be expressed as follows:

$$y = R(x) + \epsilon,$$

where ϵ is the measurement error including electronic noise, quantum noise, scatter, and patient motion artifacts [45]. The goal of CT image reconstruction is to recover an estimate of x given the projection data y and knowledge of the system matrix R . We focus in particular on the case of LDCT reconstruction, where the projection data y is obtained using a low radiation dose. The challenge in this case is that, the lower the radiation dose the higher is the noise level in the projection data y , and because the inversion of R is ill-posed, the noise is amplified in the reconstruction process.

2.2 The Two-Stage Approach

We employ a two-stage approach for CT image reconstruction. The first stage involves an initial reconstruction

using the FBP method, which is an established analytical technique for CT image reconstruction, but known to amplify measurement noise. The second stage, the CT image enhancement stage, consists of a neural network G_θ that maps the low-dose FBP-reconstructed image to an enhanced image. Mathematically, the two stage approach can be represented as follows:

$$\hat{x} = G_\theta \circ \text{FBP}(y). \quad (1)$$

where G_θ is a neural network with trainable parameters θ , FBP denotes the FBP and \hat{x} the final reconstruction result.

In our approach, as G_θ , we employ a DRUNet pretrained for Gaussian denoising of natural grayscale images, i.e., of non-CT-type data. Subsequently, we perform fine-tuning on the DRUNet for the specific downstream task of enhancing CT images, utilizing pairs of LDCT images and their corresponding NDCT counterparts. Figure 1 provides an overview; the intricacies of this method are detailed in the following subsections.

2.3 Pretraining Task: Gaussian Denoising

The pretraining task involves Gaussian denoising, utilizing pretrained weights from Zhang et al.’s DRUNet model [17]. DRUNet was originally designed for a Plug-and-Play framework. It integrates the efficiency of UNets for image-to-image translation with ResNets’ augmented modeling capacity via stacked residual blocks. The details reveal a design with four scales, each featuring identity skip connections, 2×2 strided convolution downscaling, and 2×2 transposed convolution upscaling operations. DRUNet is a deep neural network with 64, 128, 256, and 512 channels from its first to its fourth scale. The initial and final convolutional layers, along with the strided and transposed convolutional layers, do not employ any activation function, which is inspired by the network architecture design for super-resolution outlined in [46]. The model is trained on a large-scale, diverse dataset comprising 8794 natural images derived from Berkeley segmentation, Waterloo Exploration, DIV2K, and Flick2K datasets. The optimization process involves minimizing the mean absolute error (MAE) loss between the denoised image and the ground truth, using the Adam algorithm. The model is trained separately for natural grayscale and color images and demonstrates very good performance in image denoising compared to state-of-the-art methods.

2.4 Adaptation for the Downstream Task of CT Image Enhancement

The methodology derived from Zhang et al.’s DRUNet and its predecessor FFDNet [47] involves segmenting the input image into four distinct corner parts, each processed separately through the network. Zhang et al. utilize images with identically distributed Gaussian noise, allowing for individual denoising of sub-images and recombination without noticeable artifacts at the patch boundaries.

However, our application of this strategy in CT results in artifacts (cf. Figure 2c) at the patch boundaries, showcasing a sudden shift from intense to subtle smoothing with the cropping strategy. A reason for this might be that the errors are typically not Gaussian white noise, but more involved.

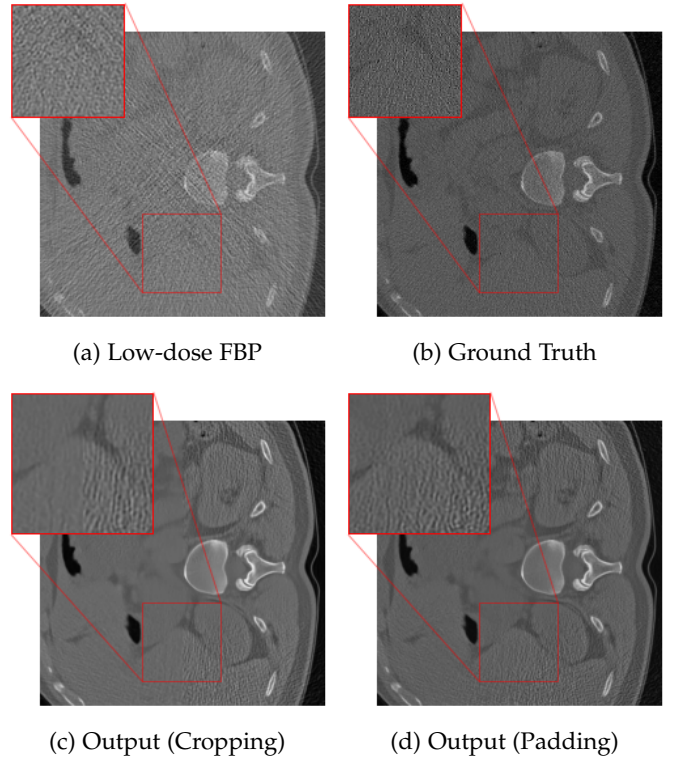


Fig. 2: An example highlighting the distinction between the Zhang et al.’s DRUNet and FFDNet methodology of cropping versus the adapted padding strategy. (a) shows the low-dose FBP, while (b) displays the corresponding ground truth. (c) highlights the artifacts at the patch boundaries resulting from denoising on sub-images, whereas (d) exhibits artifact mitigation achieved through omitting the partitioning into blocks.

For mitigating the artifacts, we modify the cropping approach of [47] by implementing padding in the output of the FBP to align with the network architecture. The DRUNet architecture operates solely on images sized as multiples of $2^4 = 16$ due to its four downsampling steps, whereas the LoDoPaB-CT dataset comprises images of size 362×362 , which does not conform to this requirement. To address this, we apply mirror padding to enlarge the images to 368×368 before passing them through the network and subsequently cropping them back to the original size of 362×362 . Figure 2 illustrates the suitability of the proposed strategy. (We point out that the image depicted in Figure 2 represents one of the most challenging reconstructions within the dataset.)

The noise level parameter in the DRUNet’s noise level map remains constant throughout the dataset in training, validation, and testing phases. This map is uniformly filled with the standard deviation σ to align with the spatial size of the noisy image. While this element is a standard component within the DRUNet architecture, in our specific implementation, it functions as a necessary presence without dynamically contributing to the network’s adaptation to varied noise levels.

Following the underlying neural network methodology of Zhang et al. in [17], we first used the MAE loss function.

The MAE loss emphasizes pixel-wise intensity accuracy and provides a basic approach to improve CT image reconstruction. Although direct evidence is lacking, there is widespread acknowledgment that the MAE loss is more robust than the MSE loss in handling outliers [48]. The MAE loss, denoted as L_{MAE} , is given as follows:

$$L_{\text{MAE}} = \frac{1}{N} \sum_{i=1}^N |\hat{x}_i - y_i|$$

Here, N represents the total number of pixels in an image, \hat{x}_i denotes the i -th pixel of the output obtained from the neural network while y_i denotes the i -th pixel of the ground truth NDCT image.

Inspired by [10] we use a composite loss function combining the MAE loss and the Structural Similarity (SSIM) loss [49]. The SSIM measures the structural similarity between two images by taking into account statistical properties of local neighborhoods instead of pixel-wise intensity accuracy. According to [50], SSIM is more adept at capturing perceptually induced changes that are frequently overlooked by traditional metrics. This is attributed to its incorporation of perceptual psychological phenomena, including brightness and contrast masking terms. To promote stability and generalization, we also incorporate L_2 regularization into the training process. The resulting regularized SSIM-based loss function L can be expressed by the following formula:

$$L = L_{\text{MAE}} + \alpha(1 - \text{SSIM}) + \lambda \|\theta\|_2^2 \quad (2)$$

The calculation of SSIM follows the methodology outlined in [49], addressing both structural and perceptual similarity between images. The parameter $\alpha > 0$ determines the weight of the $(1 - \text{SSIM})$ term. Additionally, $\|\theta\|_2^2$ represents the squared L_2 norm of the model parameters and $\lambda > 0$ denotes the regularization hyperparameter.

3 EXPERIMENTS

3.1 Experimental Setup

A. Implementation Details. For training our model, we employed the ADAM optimizer [51]. The hyperparameters β_1 and β_2 in the ADAM algorithm were set to their default values of 0.9 and 0.999, respectively, balancing the gradient and squared gradient moving averages. If not stated differently, we set the parameters α to 5 and λ to 10^{-5} . Additionally, for the learning rate strategy, an initial value of 10^{-4} was chosen, and it was halved after every 32nd epoch during our training, which lasted 264 epochs. This approach aimed to progressively fine-tune the model throughout the training process. Our implementation was realized using Python 3.9.16, and the PyTorch 2.0.0 library served as the foundational framework for our algorithm. In both the training and testing phases, we utilized an NVIDIA A40 GPU equipped with 40 GB RAM.

We employ two types of data augmentation to enhance the robustness of our network. The first method involves rotating the input and ground truth images in all four major directions. This step aims to establish network equivariance, ensuring robustness to these transformations. The second augmentation technique involves the addition of Gaussian noise to the training images. More precisely, the entire dataset is utilized in two ways: initially in its original state,

and subsequently, with the addition of 1% Gaussian noise to the input images. By augmenting the training data with synthetic noise, we expose the network to a wider spectrum of noise patterns, enabling it to learn to distinguish between inherent anatomical structures and noise-induced artifacts.

B. The LoDoPaB-CT Dataset. The LoDoPaB-CT dataset [21] comprises over 40000 pairs of human chest CT images and their corresponding simulated low-dose measurements. These images are sourced from a spectrum of imaging scenarios, providing a robust benchmark for assessing the effectiveness of our approach under varying conditions. The dataset’s ground truth images are derived from the LIDC/IDRI dataset [52], specifically cropped to dimensions of 362×362 pixels. In [26] various deep learning-based image reconstruction algorithms were systematically evaluated on the LoDoPaB-CT dataset. This renders the dataset an established and recognized benchmark for quantitatively comparing different approaches in the context of LDCT reconstruction.

C. Training Data for Fine-Tuning. For the fine-tuning of our model, we trained it on the LoDoPaB-CT dataset, following the default dataset split recommended in [26]. This dataset is split into distinct sets: 35820 training samples, 3522 validation samples, 3553 test samples, and 3678 samples for the challenge phase. The ground truth images of the challenge dataset remain confidential and are exclusively used for evaluation via the LoDoPaB-CT challenge’s online submission system (cf. <https://lodopab.grand-challenge.org>).

D. Evaluation Metrics. We utilize the metrics proposed in the LoDoPaB-CT challenge [21], which are the following four metrics: peak signal-to-noise ratio (PSNR) and structural similarity (SSIM), as well as their corresponding fixed range (FR) variants, PSNR-FR and SSIM-FR, which adopt a fixed range rather than the difference between the highest and lowest values in the ground truth image. PSNR quantifies the ratio between the maximum signal intensity and noise affecting visualization [53]. The SSIM introduced by [49] measures the structural similarity between two images, as described in Section 2.4. In all metrics, a higher value indicates a better reconstruction quality.

3.2 Experimental Results

The networks in the subsequent experiments are trained using the LoDoPaB-CT *training* dataset and evaluated on the LoDoPaB-CT *test* dataset, unless specified otherwise.

A. Effectiveness of the Rotational Augmentation.

To evaluate the impact of rotational augmentation, we conducted an experiment by training two networks: one with rotational augmentation and the other without. The objective was to investigate the network’s response to input images under different orientations. Specifically, we applied two scenarios: firstly, inputting images as they are, and secondly, rotating them by 90° before feeding them into the networks. Results depicted in Fig. 3 illustrate a noteworthy observation. For the network with rotational augmentation during training (cf. 3e and 3f), the output remains consistent regardless of the input image’s orientation. However, for the network trained without rotational augmentation (cf. 3c and 3d), the output varies between the normal and rotated

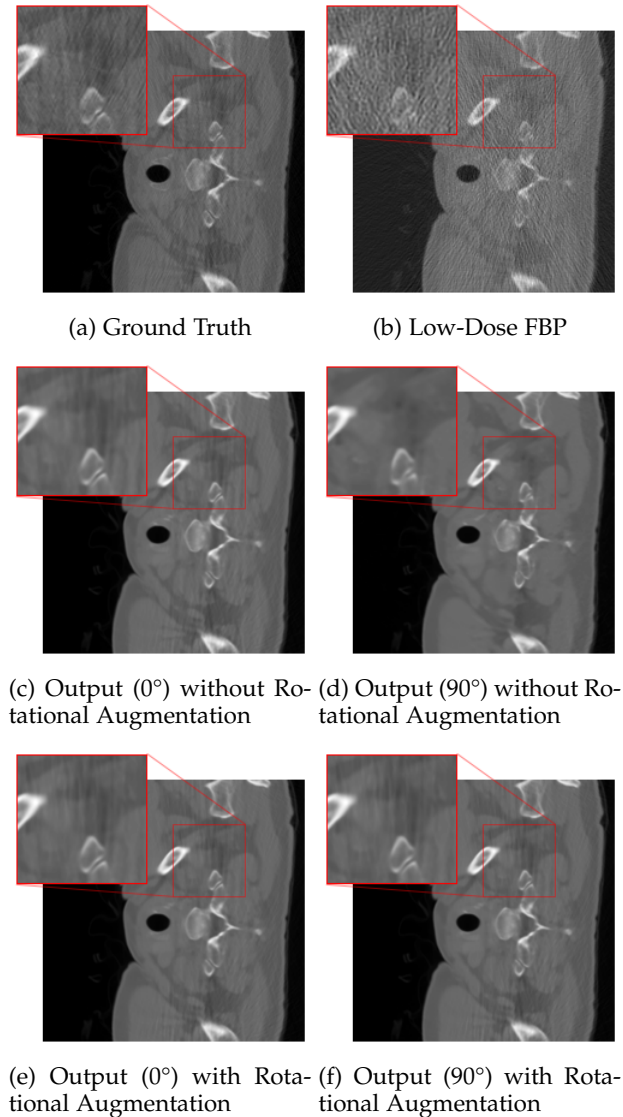


Fig. 3: Comparison of network performance with and without rotational augmentation on the LoDoPaB-CT *test* dataset. The outputs for the network with rotational augmentation remain consistent (e, f), regardless of the input image’s orientation (0° and 90°). In contrast, the network without rotational augmentation shows variation in output between normal and rotated input scenarios (c, d).

input scenarios. This experiment highlights the effectiveness of rotational augmentation in achieving network equivariance and ensuring consistent performance across different orientations of input images.

B. Effectiveness of Gaussian Noise Augmentation. In continuation of our augmentation strategy, we introduce an experiment aimed at evaluating the influence of Gaussian noise augmentation on network performance. The experiment involved a comparative analysis of three scenarios: 1) Using the dataset without Gaussian noise augmentation. 2) Employing the entire dataset in two ways: one without noise and one with 1% Gaussian noise. 3) Utilizing the entire dataset in three ways: one without noise, one with 0.5% Gaussian noise, and one with 1% Gaussian noise. The results based on

	PSNR	SSIM
Experiment 1	35.88 ± 4.709	0.8463 ± 0.1515
Experiment 2	35.91 ± 4.750	0.8466 ± 0.1513
Experiment 3	35.86 ± 4.767	0.8457 ± 0.1520

TABLE 1: Performance comparison of PSNR and SSIM metrics on the LoDoPaB-CT *test* dataset between 1) using the dataset without Gaussian noise augmentation, 2) employing the entire dataset in two ways: one without noise and one with 1% Gaussian noise and 3) utilizing the entire dataset in three ways: one without noise, one with 0.5% Gaussian noise, and one with 1% Gaussian noise.

	PSNR	SSIM
UNet with FBP using Hann filter	36.13 ± 4.901	0.8514 ± 0.1471
UNet with FBP using Ram-Lak filter	36.23 ± 4.894	0.8528 ± 0.1463

TABLE 2: Performance comparison of PSNR and SSIM metrics on the LoDoPaB-CT *test* dataset between our UNet trained on FBP reconstructions using the Hann filter and the Ram-Lak filter.

PSNR and SSIM, presented in Table 1, reveal that the methodology employed in Experiment 2 exhibited slightly better performance compared to the other two cases.

C. Impact of the Filter Type for the FBP Preprocessing. Another important aspect of the implementation involves the selection of the filter function employed in the FBP reconstruction process. We conducted experiments using two well-known filter types: the Hann filter and the Ram-Lak filter. The evaluation results are presented in Table 2. Analysis of the outcomes leads to the conclusion that the Ram-Lak filter is the preferable choice for this specific configuration. This preference is attributed to the behavior of the filters; the Hann filter, by attenuating high frequencies, induces greater blurriness in the resulting FBP compared to the Ram-Lak filter, which solely considers the absolute value. The reconstruction of a slightly blurry image poses a more challenging task for the DRUNet.

D. Hyperparameter Tuning for the SSIM-based Loss Function. To optimize the performance of our model, we turn our attention to fine-tuning the parameter α within the SSIM-based loss function. The parameter α regulates the trade-off between SSIM and MAE during the loss computation. Based on empirical values from unrecorded previous tests, we identified $\alpha = 5$ as a good choice. After various adjustments, we wanted to verify the parameter value again with a small ablation study. To save computation time for the parameter verification, we conducted preliminary experiments on a subset of the LoDoPaB-CT *training* dataset, comprising 640 images out of the total 35820, training for 400 epochs. The results for different values of α are presented in Table 3. The results emphasize that there is minimal variation across different positive α values. To emphasize the importance of balancing SSIM and MAE, we also set α to 0, relying solely on MAE loss with L_2 regularization. This approach resulted in a notable decline in performance. Conversely, it is evident that higher α values gradually result in reduced model performance.

α	PSNR	SSIM
0	35.44 ± 4.528	0.8347 ± 0.1583
1	35.94 ± 4.729	0.8470 ± 0.1511
3	35.94 ± 4.750	0.8471 ± 0.1510
5	35.91 ± 4.750	0.8466 ± 0.1513
7	35.88 ± 4.748	0.8462 ± 0.1515
10	35.86 ± 4.747	0.8460 ± 0.1516

TABLE 3: Results of tuning α on a small scale experiment using 640 images from the LoDoPaB-CT *training* dataset, with evaluation conducted on the entire LoDoPaB-CT *test* dataset.

α	PSNR	SSIM
3	36.18 ± 4.858	0.8518 ± 0.1470
5	36.23 ± 4.894	0.8528 ± 0.1463

TABLE 4: Results of tuning α on the entire LoDoPaB-CT training dataset, confirming that $\alpha = 5$ provides better performance.

To further investigate this hyperparameter choice, we performed an additional experiment on the complete LoDoPaB-CT dataset. We compared our initial setting of $\alpha = 5$ to the best performing value observed in the small scale experiment, $\alpha = 3$. The outcomes are presented in Table 4. The results reveal that in this specific experiment $\alpha = 5$ performs better than $\alpha = 3$, suggesting an enhanced overall reconstruction quality. Given these results, we have chosen to use $\alpha = 5$ as the preferred parameter setting for our SSIM-based loss function.

E. Effectiveness of the Pretraining/Fine-Tuning. To demonstrate the effectiveness of fine-tuning the pretrained network, we conduct a comparative analysis between the proposed method and a network trained using the identical architecture but with randomly initialized weights. Table 5 presents the PSNR and SSIM values, where “Second stage based on fine-tuning” refers to the proposed approach, and “Second stage from scratch” refers to the network trained from scratch. The results demonstrate a notable improvement, particularly in the PSNR, when we fine-tune the pretrained network.

Figure 4 provides visual insights into the reconstruction process. It showcases results for three test samples from the LoDoPaB-CT *test* dataset. The first column displays the ground truth, while the second column showcases the outcome of the low-dose FBP, serving as the initial stage in our method. The subsequent stage enhances the FBP result using a DRUNet, which is depicted in the third and fourth columns. The third column illustrates the enhanced result

	PSNR	SSIM
Second stage from scratch	35.47 ± 5.073	0.8408 ± 0.1499
Second stage based on fine-tuning (proposed)	36.23 ± 4.894	0.8528 ± 0.1463

TABLE 5: Performance comparison w.r.t. PSNR and SSIM metrics on the LoDoPaB-CT *test* dataset between the DRUNet architecture trained from scratch and utilizing fine-tuning on the pretrained DRUNet.

when the DRUNet architecture is trained from scratch, while the fourth column portrays the enhanced result obtained with fine-tuning the pretrained DRUNet. It is evident from the visualizations that the proposed two-stage method consistently enhances basic FBP results. Moreover, working with fine-tuning yields slightly better metrics, as evidenced by improvements in PSNR and SSIM. These observations are in line with the quantitative findings presented in Table 5.

F. LoDoPaB-CT Challenge Results. We evaluated the proposed method within the LoDoPaB-CT challenge, where it demonstrated noteworthy performance. In the latest standings, as documented on the challenge platform (<https://lodopab.grand-challenge.org/evaluation/challenge/leaderboard>), our approach has achieved a shared first position alongside ItNet. Our method attains the highest rank in the SSIM metric, however, ItNet exhibits a slight advantage in the other three metrics. We employ the model as described in Paragraph 3.1 A, including rotational augmentation, Gaussian noise augmentation, and the Ram-Lak filter for FBP. The initial version was trained on the LoDoPaB-CT *training* dataset, while the second version underwent an additional fine-tuning process. In this fine-tuning step, we utilized identical parameters and fine-tuned the network from the first version on the complete LoDoPaB-CT dataset, encompassing training, testing, and validation subsets. It is noteworthy to emphasize that a subset of only 271 images was exclusively reserved for testing purposes before the official leaderboard submission. For a detailed comparison of our method and others, including references to corresponding papers, we provide a comprehensive overview in Table 6.

4 CONCLUSION

In this paper, we have introduced a two-stage approach for LDCT image reconstruction using classical FBP reconstruction in the first stage and a deep learning method in the second stage for CT image enhancement. The key innovation lies in the training strategy: first, the neural network is pretrained on a different task, namely Gaussian noise removal from natural grayscale images; then, it is fine-tuned for the downstream task of LDCT image enhancement. In particular, we deviate from common practice of using domain-specific CT data for pretraining.

We evaluated the proposed approach at the LoDoPaB-CT challenge. The proposed method achieved a joint first place together with ItNet [20]. Our method has the highest rank in the SSIM metric, and ItNet has a slight edge in the other three metrics, namely PSNR, PSNR-FR and SSIM-FR. The proposed method is structurally simpler than ItNet, as it does not require an iterative refinement step. From a point of view of computational efficiency, the proposed method only requires performing a FBP plus one forward pass of the network. In conclusion, the method is computationally efficient and maintains competitive performance.

To validate the effectiveness of the proposed fine-tuning strategy, we compared to a network trained from scratch with identical architecture (DRUNet architecture). The results show the advantage by yielding improvements with respect to both PSNR and SSIM.

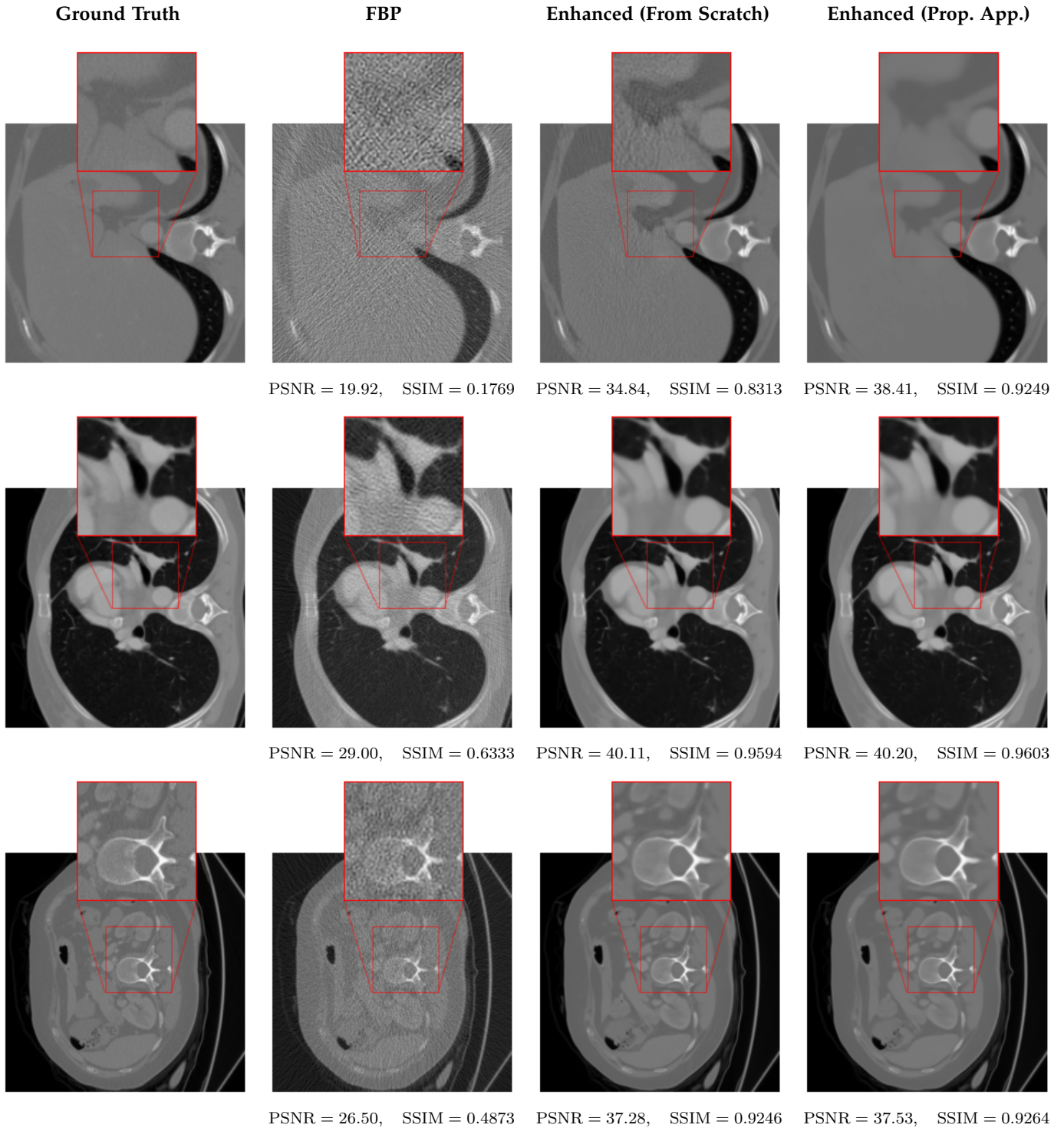


Fig. 4: Reconstruction results for three test samples from the LoDoPaB-CT *test* dataset. The first column shows the ground truth while the second column shows the results of the FBP. FBP is applied in the first stage of our method. The second stage enhances the FBP result using a DRUNet. The third column shows the enhanced results, when the DRUNet architecture is trained from scratch. In the fourth column the enhanced results are obtained by employing the proposed approach, specifically through the process of fine-tuning the pretrained DRUNet. The proposed two-stage method is generally able to enhance basic FBP results, while working with the pretrained DRUNet yields slightly better metrics (PSNR and SSIM).

	Mean Position	PSNR	PSNR-FR	SSIM	SSIM-FR
FBP	53	30.19 ± 2.555	34.46 ± 2.182	0.7274 ± 0.1273	0.8356 ± 0.08497
TV	47.5	33.36 ± 2.736	37.63 ± 2.702	0.8303 ± 0.1211	0.9030 ± 0.08196
CINN [41]	33.8	35.54 ± 3.509	39.81 ± 3.477	0.8542 ± 0.1215	0.9189 ± 0.08143
UNet++ [18]	30	35.37 ± 3.361	39.64 ± 3.404	0.8609 ± 0.1192	0.9225 ± 0.08007
MS-D-CNN [27]	29.3	35.85 ± 3.601	40.12 ± 3.557	0.8576 ± 0.1221	0.9210 ± 0.08161
Original UNet [28]	27	35.87 ± 3.593	40.14 ± 3.566	0.8592 ± 0.1200	0.9218 ± 0.08021
LoDoPaB UNet [26]	19.3	36.00 ± 3.631	40.28 ± 3.590	0.8618 ± 0.1185	0.9233 ± 0.07912
MUSC [23]	15.5	36.08 ± 3.682	40.35 ± 3.644	0.8628 ± 0.1193	0.9238 ± 0.07957
ISTA UNet [19]	15.3	36.09 ± 3.687	40.36 ± 3.648	0.8623 ± 0.1197	0.9236 ± 0.07969
Learned P-D. [22]	10.5	36.25 ± 3.696	40.52 ± 3.635	0.8662 ± 0.1152	0.9260 ± 0.07635
ItNet [20]	1.8	36.47 ± 3.791	40.74 ± 3.743	<i>0.8692 ± 0.1150</i>	0.9275 ± 0.07632
Our method	1.8	<i>36.43 ± 3.894</i>	<i>40.70 ± 3.867</i>	0.8700 ± 0.1162	<i>0.9274 ± 0.07819</i>

TABLE 6: Evaluation of our method on the LoDoPaB-CT *challenge* dataset, compared to various state-of-the-art methods. The metrics are taken from [21]. Mean Position, in this context, refers to the average placement across the four distinct positions on the leaderboard concerning the four evaluation metrics. The results are taken from the challenge platform (<https://lodopab.grand-challenge.org/evaluation/challenge/leaderboard>) on March 4, 2024. The highest overall score is emphasized in boldface, while the second-best score is highlighted in italic.

We investigated different design choices and hyperparameter settings. The use of a regularized SSIM-based loss function performed better than a model trained with only MAE loss, highlighting the importance of incorporating SSIM. Further, padding the FBP output, instead of cropping, mitigated visual artifacts. Including rotational augmentation proved to give more consistent results across different image orientations. Experiments with Gaussian noise augmentation improved performance compared to setups without such augmentation. Finally, employing the Ram-Lak filter demonstrated slightly better performance compared to the Hann filter. We believe that this is because of the preservation of high frequencies which better aligns with the DRUNet’s reconstruction process.

One topic of future research consists of the application of the proposed approach to other imaging modalities. The proposed method relies on CT via the FBP which provides a (regularized) inversion of the corresponding imaging operator as well as via the dataset. Replacing CT by another imaging modality thus requires modifying the reconstruction method as well as a data set for fine-tuning. Another topic can be increasing the size of the datasets for pretraining and the size of the network architecture. Following the observation in Computer Vision that large networks trained on large datasets provide an improved basis for performing downstream tasks, we believe that this strategy can further improve the reconstruction quality.

ACKNOWLEDGMENTS

T. S., T. M. and A. W. acknowledge support by the Hessian Ministry of Higher Education, Research, Science, and the Arts through the “Programm zum Aufbau eines akademischen Mittelbaus an hessischen Hochschulen”. M. S. acknowledges support by the project DIBCO funded by the research program “Informations- und Kommunikationstechnik” of the Bavarian State Ministry of Economic Affairs, Regional Development and Energy (DIK-2105-0044 / DIK0264). A. W. acknowledges support of Deutsche Forschungsgemeinschaft (DFG) under project number 514177753.

REFERENCES

- [1] M. Lell, J. Wildberger, H. Alkadhi, J. Damlakis, and M. Kachelriess, “Evolution in Computed Tomography: The Battle for Speed and Dose,” *Investigative Radiology*, vol. 50, no. 9, pp. 629–644, 2015.
- [2] W. A. Kalender, *Computed Tomography: Fundamentals, System Technology, Image Quality, Applications*. John Wiley & Sons, 2011.
- [3] Q. Yang, P. Yan, Y. Zhang, H. Yu, Y. Shi, X. Mou, M. K. Kalra, Y. Zhang, L. Sun, and G. Wang, “Low-Dose CT Image Denoising Using a Generative Adversarial Network With Wasserstein Distance and Perceptual Loss,” *IEEE Transactions on Medical Imaging*, vol. 37, no. 6, pp. 1348–1357, 2018.
- [4] S. Lu, B. Yang, Y. Xiao, S. Liu, M. Liu, L. Yin, and W. Zheng, “Iterative reconstruction of low-dose CT based on differential sparse,” *Biomedical Signal Processing and Control*, vol. 79, p. 104204, 2023.
- [5] Y. Hu, Z. Zheng, H. Yu, J. Wang, X. Yang, and H. Shi, “Ultra-low-dose CT reconstructed with the artificial intelligence iterative reconstruction algorithm (AIIR) in 18F-FDG total-body PET/CT examination: a preliminary study,” *EJNMMI Physics*, vol. 10, no. 1, p. 1, 2023.
- [6] S. Kulathilake, N. Abdullah, A. Sabri, and K. W. Lai, “A review on Deep Learning approaches for low-dose Computed Tomography restoration,” *Complex & Intelligent Systems*, vol. 9, 2021.
- [7] H. Li *et al.*, “Transformer With Double Enhancement for Low-Dose CT Denoising,” *IEEE Journal of Biomedical and Health Informatics*, vol. 27, no. 10, pp. 4660–4671, 2023.
- [8] D. Wang, F. Fan, Z. Wu, R. Liu, F. Wang, and H. Yu, “CTformer: convolution-free Token2Token dilated vision transformer for low-dose CT denoising,” *Physics in Medicine and Biology*, vol. 68, 2023.
- [9] F. N. Mazandarani, P. Babyn, and J. Alirezaie, “UNeXt: a Low-Dose CT denoising UNet model with the modified ConvNeXt block,” in *ICASSP 2023 - 2023 IEEE International Conference on Acoustics, Speech and Signal Processing (ICASSP)*, 2023, pp. 1–5.
- [10] L. Xiong, N. Li, W. Qiu, and Y. Zhang, “Re-UNet: A Novel Multi-scale Reverse U-shaped Network Architecture for Low-dose CT Image Reconstruction,” *Available at SSRN 4426158*, 2023.
- [11] Y. Liu, J. Ma, Y. Fan, and Z. Liang, “Adaptive-weighted total variation minimization for sparse data toward low-dose x-ray computed tomography image reconstruction,” *Physics in Medicine and Biology*, vol. 57, pp. 7923–7956, 2012.
- [12] S. Niu, Y. Gao, Z. Bian, J. Huang, W. Chen, G. Yu, Z. Liang, and J. Ma, “Sparse-view x-ray CT reconstruction via total generalized variation regularization,” *Physics in Medicine & Biology*, vol. 59, no. 12, p. 2997, 2014.
- [13] L. Liu, X. Li, K. Xiang, J. Wang, and S. Tan, “Low-Dose CBCT Reconstruction Using Hessian Schatten Penalties,” *IEEE Transactions on Medical Imaging*, vol. 36, no. 12, pp. 2588–2599, 2017.
- [14] G. Litjens, T. Kooi, B. E. Bejnordi, A. A. A. Setio, F. Ciompi, M. Ghafoorian, J. A. Van Der Laak, B. Van Ginneken, and C. I. Sánchez, “A survey on deep learning in medical image analysis,” *Medical Image Analysis*, vol. 42, pp. 60–88, 2017.

- [15] W. Stiller, "Basics of iterative reconstruction methods in computed tomography: a vendor-independent overview," *European Journal of Radiology*, vol. 109, pp. 147–154, 2018.
- [16] D. H. Ye, S. Srivastava, J.-B. Thibault, K. Sauer, and C. Bouman, "Deep Residual Learning for Model-Based Iterative CT Reconstruction Using Plug-and-Play Framework," in *2018 IEEE International Conference on Acoustics, Speech and Signal Processing (ICASSP)*, 2018, pp. 6668–6672.
- [17] K. Zhang, Y. Li, W. Zuo, L. Zhang, L. Van Gool, and R. Timofte, "Plug-and-Play Image Restoration With Deep Denoiser Prior," *IEEE Transactions on Pattern Analysis and Machine Intelligence*, vol. 44, no. 10, pp. 6360–6376, 2022.
- [18] Z. Zhou, M. M. Rahman Siddiquee, N. Tajbakhsh, and J. Liang, "Unet++: A Nested U-Net Architecture for Medical Image Segmentation," in *Deep Learning in Medical Image Analysis and Multimodal Learning for Clinical Decision Support: 4th International Workshop, DLMIA 2018, and 8th International Workshop, ML-CDS 2018, Held in Conjunction with MICCAI 2018, Granada, Spain, September 20, 2018, Proceedings 4*. Springer, 2018, pp. 3–11.
- [19] T. Liu, A. Chaman, D. Belius, and I. Dokmanić, "Interpreting U-Nets via Task-Driven Multiscale Dictionary Learning," *ArXiv*, 2020.
- [20] M. Genzel, I. Gühring, J. Macdonald, and M. März, "Near-Exact Recovery for Tomographic Inverse Problems via Deep Learning," in *Proceedings of the 39th International Conference on Machine Learning*, vol. PMLR 162, 2022, pp. 7368–7381.
- [21] J. Leuschner, M. Schmidt, P. S. Ganguly, V. Andriiashen, S. B. Coban, A. Denker, D. F. Bauer, A. Hadjifaradji, K. J. Batenburg, P. Maass, and M. van Eijnatten, "Quantitative Comparison of Deep Learning-Based Image Reconstruction Methods for Low-Dose and Sparse-Angle CT Applications," *Journal of Imaging*, vol. 7, 2021.
- [22] J. Adler and O. Öktem, "Learned Primal-Dual Reconstruction," *IEEE Transactions on Medical Imaging*, vol. 37, no. 6, pp. 1322–1332, 2018.
- [23] T. Liu, A. Chaman, D. Belius, and I. Dokmanic, "Learning Multiscale Convolutional Dictionaries for Image Reconstruction," *IEEE Transactions on Computational Imaging*, vol. 8, pp. 1–1, 2022.
- [24] A. Radford, K. Narasimhan, T. Salimans, and I. Sutskever, "Improving Language Understanding by Generative Pre-Training," 2018. [Online]. Available: https://s3-us-west-2.amazonaws.com/openai-assets/research-covers/language-unsupervised/language_understanding_paper.pdf
- [25] Z. Liu, H. Hu, Y. Lin, Z. Yao, Z. Xie, Y. Wei, J. Ning, Y. Cao, Z. Zhang, L. Dong et al., "Swin transformer v2: Scaling up capacity and resolution," in *Proceedings of the IEEE/CVF Conference on Computer Vision and Pattern Recognition*, 2022, pp. 12 009–12 019.
- [26] J. Leuschner, M. Schmidt, D. O. Bagger, and P. Maass, "LoDoPaB-CT, a benchmark dataset for low-dose computed tomography reconstruction," *Scientific Data*, vol. 8, no. 1, p. 109, 2021.
- [27] D. M. Pelt, K. J. Batenburg, and J. A. Sethian, "Improving tomographic reconstruction from limited data using mixed-scale dense convolutional neural networks," *Journal of Imaging*, vol. 4, no. 11, p. 128, 2018.
- [28] O. Ronneberger, P. Fischer, and T. Brox, "U-net: Convolutional networks for biomedical image segmentation," in *Medical Image Computing and Computer-Assisted Intervention—MICCAI 2015: 18th International Conference, Munich, Germany, October 5–9, 2015, Proceedings, Part III 18*. Springer, 2015, pp. 234–241.
- [29] Z. Zhang, Q. Liu, and Y. Wang, "Road extraction by deep residual U-net," *IEEE Geoscience and Remote Sensing Letters*, vol. 15, no. 5, pp. 749–753, 2018.
- [30] X. Wu, D. Hong, and J. Chanussot, "UIU-Net: U-Net in U-Net for Infrared Small Object Detection," *IEEE Transactions on Image Processing*, vol. 32, pp. 364–376, 2023.
- [31] A. Jansson, E. Humphrey, N. Montecchio, R. Bittner, A. Kumar, and T. Weyde, "Singing voice separation with deep U-Net convolutional networks," in *Proceedings of the 18th International Society for Music Information Retrieval Conference*, Suzhou, China, 2017.
- [32] H. Chen, Y. Zhang, M. K. Kalra, F. Lin, Y. Chen, P. Liao, J. Zhou, and G. Wang, "Low-Dose CT With a Residual Encoder-Decoder Convolutional Neural Network," *IEEE Transactions on Medical Imaging*, vol. 36, no. 12, pp. 2524–2535, 2017.
- [33] J. Kim, J. Kim, G. Han, C. Rim, and H. Jo, "Low-dose CT Image Restoration using generative adversarial networks," *Informatics in Medicine Unlocked*, vol. 21, p. 100468, 2020.
- [34] J. M. Wolterink, T. Leiner, M. A. Viergever, and I. Išgum, "Generative Adversarial Networks for Noise Reduction in Low-Dose CT," *IEEE Transactions on Medical Imaging*, vol. 36, no. 12, pp. 2536–2545, 2017.
- [35] H. Shan, Y. Zhang, Q. Yang, U. Kruger, M. K. Kalra, L. Sun, W. Cong, and G. Wang, "3-D Convolutional Encoder-Decoder Network for Low-Dose CT via Transfer Learning From a 2-D Trained Network," *IEEE Transactions on Medical Imaging*, vol. 37, no. 6, pp. 1522–1534, 2018.
- [36] Z. Hu, C. Jiang, F. Sun, Q. Zhang, Y. Ge, Y. Yang, X. Liu, H. Zheng, and D. Liang, "Artifact correction in low-dose dental CT imaging using Wasserstein generative adversarial networks," *Medical Physics*, vol. 46, p. 1686–1696, 2019.
- [37] X. Yi and P. Babyn, "Sharpness-Aware Low-Dose CT Denoising Using Conditional Generative Adversarial Network," *Journal of Digital Imaging*, vol. 31, 2017.
- [38] F. Fan, H. Shan, M. K. Kalra, R. Singh, G. Qian, M. Getzin, Y. Teng, J. Hahn, and G. Wang, "Quadratic Autoencoder (Q-AE) for Low-Dose CT Denoising," *IEEE Transactions on Medical Imaging*, vol. 39, no. 6, pp. 2035–2050, 2020.
- [39] Y. Ma, B. Wei, P. Feng, P. He, X. Guo, and G. Wang, "Low-dose CT image denoising using a generative adversarial network with a hybrid loss function for noise learning," *IEEE Access*, vol. 8, pp. 67 519–67 529, 2020.
- [40] T. Liang, Y. Jin, Y. Li, and T. Wang, "EDCNN: Edge enhancement-based Densely Connected Network with Compound Loss for Low-Dose CT Denoising," in *2020 15th IEEE International Conference on Signal Processing (ICSP)*, vol. 1, 2020, pp. 193–198.
- [41] A. Denker, M. Schmidt, J. Leuschner, P. Maass, and J. Behrmann, "Conditional normalizing flows for low-dose computed tomography image reconstruction," *arXiv:2006.06270*, 2020.
- [42] E. Kang, J. Min, and J. C. Ye, "A deep convolutional neural network using directional wavelets for low-dose X-ray CT reconstruction," *Medical Physics*, vol. 44, p. e360–e375, 2016.
- [43] M. Gholizadeh-Ansari, J. Alirezaie, and P. Babyn, "Low-dose CT Denoising Using Edge Detection Layer and Perceptual Loss," in *2019 41st Annual International Conference of the IEEE Engineering in Medicine and Biology Society (EMBC)*, 2019, pp. 6247–6250.
- [44] S. J. Kisner, E. Haneda, C. A. Bouman, S. Skatter, M. Kourinny, and S. Bedford, "Model-based CT reconstruction from sparse views," in *Second International Conference on Image Formation in X-Ray Computed Tomography*, 2012, pp. 444–447.
- [45] M. Sandborg, *Computed Tomography: Physical principles and biohazards*. Linköping University Electronic Press, 1995.
- [46] B. Lim, S. Son, H. Kim, S. Nah, and K. Mu Lee, "Enhanced deep residual networks for single image super-resolution," in *Proceedings of the IEEE Conference on Computer Vision and Pattern Recognition Workshops*, 2017, pp. 136–144.
- [47] K. Zhang, W. Zuo, and L. Zhang, "FFDNet: Toward a Fast and Flexible Solution for CNN-Based Image Denoising," *IEEE Transactions on Image Processing*, vol. 27, no. 9, pp. 4608–4622, 2018.
- [48] C. Bishop, *Pattern recognition and machine learning*. Springer, 2011.
- [49] Z. Wang, A. Bovik, H. Sheikh, and E. Simoncelli, "Image quality assessment: from error visibility to structural similarity," *IEEE Transactions on Image Processing*, vol. 13, no. 4, pp. 600–612, 2004.
- [50] D. R. I. M. Setiadi, "PSNR vs SSIM: imperceptibility quality assessment for image steganography," *Multimedia Tools and Applications*, vol. 80, pp. 1–22, 2021.
- [51] D. P. Kingma and J. Ba, "Adam: A method for stochastic optimization," *arXiv:1412.6980*, 2014.
- [52] S. G. Armato III, G. McLennan, L. Bidaut, M. F. McNitt-Gray, C. R. Meyer, A. P. Reeves, B. Zhao, D. R. Aberle, C. I. Henschke, E. A. Hoffman et al., "The lung image database consortium (LIDC) and image database resource initiative (IDRI): a completed reference database of lung nodules on CT scans," *Medical Physics*, vol. 38, no. 2, pp. 915–931, 2011.
- [53] U. Sara, M. Akter, and M. S. Uddin, "Image Quality Assessment through FSIM, SSIM, MSE and PSNR—A Comparative Study," *Journal of Computer and Communications*, vol. 07, pp. 8–18, 2019.